01 Jul 2022

Room-Temperature Mechanical Properties of a High-Entropy Diboride

Alec C. Murchie

Jeremy Lee Watts
Missouri University of Science and Technology, jwatts@mst.edu

William Fahrenholtz
Missouri University of Science and Technology, billf@mst.edu

Gregory E. Hilmas
Missouri University of Science and Technology, ghilmas@mst.edu

Recommended Citation

A. C. Murchie et al., "Room-Temperature Mechanical Properties of a High-Entropy Diboride," *International Journal of Applied Ceramic Technology*, vol. 19, no. 4, pp. 2293 - 2299, Wiley, Jul 2022.
The definitive version is available at https://doi.org/10.1111/ijac.14026

Received: 3 November 2021 | Revised: 13 January 2022 | Accepted: 18 January 2022

DOI: 10.1111/ijac.14026

International Journal of Applied Ceramic Technology

RESEARCH ARTICLE

Room-temperature mechanical properties of a high-entropy diboride

Alec C. Murchie | **Jeremy L. Watts** | **William G. Fahrenholtz** | **Gregory E. Hilmas**

Department of Materials Science and Engineering, Missouri University of Science and Technology, Rolla, Missouri, USA

Correspondence
Gregory E. Hilmas, Materials Science & Engineering, Missouri University of Science and Technology, 220 McNutt Hall, Rolla, MO 65409-0340, USA.
Email: ghilmas@mst.edu

Abstract

The mechanical properties of a (Hf,Mo,Nb,Ta,W,Zr)B_2 high-entropy ceramic were measured at room temperature. A two-step synthesis process was utilized to produce the (Hf,Mo,Nb,Ta,W,Zr)B_2 ceramics. The process consisted of a boro/carbothermal reduction reaction followed by solid solution formation and densification through spark plasma sintering. Nominally, phase pure (Hf,Mo,Nb,Ta,W,Zr)B_2 was sintered to near full density (8.98 g/cm^3) at 2000°C. The mean grain size was 6 ± 2 μm with a maximum grain size of 17 μm. Flexural strength was 528 ± 53 MPa, Young's modulus was 520 ± 12 GPa, fracture toughness was 3.9 ± 1.2 MPa·m$^{1/2}$, and hardness ($HV_{0.2}$) was 33.1 ± 1.1 GPa. A Griffith-type analysis determined the strength limiting flaw to be the largest grains in the microstructure. This is one of the first reports of a variety of mechanical properties of a six-component high-entropy diboride.

KEYWORDS
borides, ceramic engineering, mechanical properties

1 | INTRODUCTION

Ultra-high temperature ceramics (UHTCs) have potential use as structural materials in extreme environments, such as on the leading and trailing edges of hypersonic vehicles. These vehicles will be traveling Mach 5 or greater and are thus expected to experience extreme temperatures (> 2000°C). A new class of UHTCs called high-entropy borides (HEBs) were recently synthesized and densified and exhibited better oxidation resistance and higher hardness than the individual diborides.[1] As such, it is of interest to learn more about the mechanical properties of HEBs.

Several different methods have been used to synthesize HEBs.[2–7] Wen et al. synthesized (Hf,Ti,Zr)B_2 and (Nb,Ta,Ti)B_2 by a molten salt synthesis method at 1100°C with 30% excess B.[4] The resulting powders had a nanorod morphology with diameters of 20–40 nm and lengths of 100–200 nm. It was also necessary to wash the powders to remove residual NaCl/KCl salts and B_2O_3. Tallarita et al. synthesized a (Hf,Mo,Nb,Ta,Ti)B_2 ceramic from elemental metal powders and boron using a self-propagating high-temperature synthesis method and then consolidated the powder by spark plasma sintering (SPS).[2] The relative density of the final ceramic reached only 92.5%. Zhang et al. synthesized powders for several HEB compositions by vacuum boro/carbothermal reduction at 1600°C and then sintering the powders by SPS at 2000°C.[6] Relative densities ranged from 96.3%–98.5%. Oxide impurities were present in the sintered specimens due to an incomplete reaction that was non-stoichiometric with respect to the desired reaction. Liu et al. synthesized a (Hf,Nb,Ta,Ti,Zr)B_2 ceramic by the borothermal reduction reaction of oxide powders and B at 1700°C under vacuum with a 2:11 oxide/B ratio.[3] The resulting powder had an average particle size of ~ 310 nm. Zhang et al. also synthesized several ((Cr,Hf,Ta,Ti,Zr)$_2$, (Hf,Mo,Nb, Ti,Zr)B_2, (Hf,Mo,Nb,Ta,Ti)B_2) HEB powders by the borothermal reduction reaction at 1600°C under vacuum.[5] Powders

were spark plasma sintered and relative densities in the range of 95%–99.2% were achieved. While various methods have been used to synthesize HEB composites, producing large amounts of high-purity powder has proven difficult. Feng et al. synthesized a (Hf,Nb,Ta,Ti,Zr)B_2 HEB powder by a two-step process method consisting of a boro/carbothermal reduction followed by solid solution formation.[7] This method produced a low-oxygen content (0.3 wt%) and a small average particle size (430 nm). Synthesis methods that allow for large-scale production of high-purity and small particle size powders are required to advance the science of HEBs.

Most reports of the mechanical behavior of HEBs have been limited to Vickers hardness or indentation fracture toughness, mechanical tests that can be made on relatively small specimens. The hardness values range from 21.0 GPa for a (Cr,Hf,Ta,Ti,Zr)B_2 HEB and 28.3 GPa for a (Cr,Hf,Ta,Ti,Zr)B_2 HEB.[1,5] HEBs containing Mo and W have demonstrated higher hardness > 30 GPa at loads < 1.96 N.[8] Fracture toughness values of HEBs are not widely reported, with most reports utilizing indentation methods. For example, Zhang reported indentation toughness values of ~ 4 MPa·$m^{1/2}$ for a few different HEB compositions.[6] However, indentation toughness values inherently have variability in the range of 10%–30%, with additional error that can be added depending on the accuracy of the Young's modulus used in the calculations. Liu reported the four-point bend strength of a fully dense (Hf,Nb,Ta,Ti,Zr)B_2 with an average grain size of 4 μm to be 339 ± 17 MPa and the fracture toughness to be 3.8 ± 0.4 MPa·$m^{1/2}$ using the single-edge notched beam technique.[9]

The objective of the present work was to produce a fully dense, six-component HEB ceramic ((Hf,Mo,Nb,Ta,W,Zr)B_2) and investigate its room temperature mechanical properties, including flexure strength, elastic modulus, hardness, and fracture toughness.

2 | PROCEDURE

2.1 | Processing

(Hf,Mo,Nb,Ta,W,Zr)B_2 ceramics were produced by a two-step synthesis method consisting of a solid-state borocarbothermal reduction (BCTR) of oxide powders and then densification and further solid solution formation and densification by SPS. The general BCTR reactions used are summarized by Reactions (1)–(3), while Reaction (4) describes the overall reaction combined with solid solution formation.

$$2MeO_2 + B_4C + 3C \rightarrow 2MeB_2 + 4CO\,(g)\,, \quad (1)$$

$$Me_2O_5 + B_4C + 4C \rightarrow 2MeB_2 + 5CO\,(g)\,, \quad (2)$$

$$2MeO_3 + B_4C + 5C \rightarrow 2MeB_2 + 6CO\,(g)\,, \quad (3)$$

$$ZrO_2 + 0.5Nb_2O_5 + MoO_3 + HfO_2 + 0.5Ta_2O_5 + WO_3 + 3B_4C + 12C \rightarrow 6\,(Hf, Mo, Nb, Ta, W, Zr)\,B_2 + 15CO\,(g)\,. \quad (4)$$

Zirconium oxide (ZrO_2; Grade KZ-0Y-LSF, KCM Corporation, Nagoya, Japan), niobium oxide (Nb_2O_5; Grade 208515, Alfa Aesar, Ward Hill, MA), molydenum oxide (MoO_3; Grade US1116M, US Research Nanomaterials, Inc, Houston, TX), hafnium oxide (HfO_2; Grade 40270, Alfa Aesar, Ward Hill, MA), tantalum oxide (Ta_2O_5; Grade 73R-0804, Inframat Advanced Materials, Manchester, CT), and tungsten oxide (WO_3; Grade 74R-0816, Inframat Advanced Materials, Manchester, CT) powders were used. The oxide powders were batched in stoichiometric ratios to achieve an equimolar composition of the HEB. The powders were attrition milled in acetone for 3 h (model HD-01, Union Process, Akron, OH) with 3 mm diameter spherical yttria-stabilized ZrO_2 media to homogenize and reduce the particle size of the mixture. Rotary evaporation (Rotavapor R-124, Buchi, Flawil, Germany) was utilized to dry the slurry at a temperature of 60°C, under vacuum (~ 16 kPa), and at a rotation speed of 60 rpm. After drying the oxide powder mixture, the mixture was then batched with 11 wt% excess boron carbide (B_4C; Grade HD 20, H.C. Starck, Newton, MA) and 4.5 wt% less than the calculated stoichiometric ratio for the carbon black (Vulcan XC72; Cabot Co., Alpharetta, GA) and ball mixed using 5 mm diameter spherical zirconia milling media for 6 h in acetone. The slurry was dried by rotary evaporation at a temperature of 60°C, under vacuum (~ 16 kPa), and at a rotation speed of 60 rpm. The dried powder was sieved through a 50 mesh screen and uniaxially pressed into a ~ 57 mm disc using a ~ 0.5 MPa load.

A graphite element furnace (Model HP50-7010G, Thermal Technology, Santa Rosa, CA) was used to react the powder compacts under vacuum (~ 13.3 Pa). The furnace was heated at 5°C/min to 660°C, held for 5 min, ramped at 1°C/min to 665°C and then held for 5 min. The slow heating process was repeated until 700°C at which time the ramp rate was increased to 5°C/min to the final reaction temperature of 1650°C. The furnace was held for 8 h and then allowed to cool at ~ 25°C/min. The reacted powder compacts were then crushed and sieved through a 50-mesh screen.

Powders were densified by SPS (Model DCS-10, Thermal Technology, Santa Rosa, CA) in a 40 mm diameter die lined with graphite foil. A 20 MPa preload was applied, and the furnace was evacuated (~ 2.67 Pa). The furnace was heated at 75°C/min to 1650°C and held for 20 min to

remove surface oxides from the powder particles.[10,11] The load was then increased to 50 MPa, and the furnace was heated to 2000°C at 50°C/min and held for 5 min. The furnace then cooled at 50°C/min to 1600°C, where the load was decreased to 5 MPa and the furnace backfilled with argon and allowed to cool.

2.2 | Characterization

A modified Archimedes' method was utilized to determine the density of the HEB billets produced by SPS. Billets were boiled in distilled water for 2 h, and then placed under mild vacuum (~16 kPa) for 30 min before measurement. Scanning electron microscopy (SEM; Raith eLine Plus, Dortmund, Germany) equipped with energy-dispersive spectroscopy (EDS; Quantax Bruker, Billerica, MA) was used to examine the microstructures. Cross-sections of billets were polished to a 0.25 μm finish. Image analysis software (ImageJ, National Institutes of Health, Bethesda, MD) was used to measure the grain sizes of the SEM images by measuring the fitted ellipse and Feret diameter based on at least 500 grains. X-ray diffraction (XRD) analysis was performed utilizing a PANalytical X-Pert Pro diffractometer (Malvern Panalytical Ltd., Royston, UK) with a Cu-Kα (radiation ($\lambda = 1.540562$ Å) X-ray source. Dense billets were crushed and ground and passed through a 200-mesh sieve. The filament current was set to 45 mA and the accelerating voltage was set to 45 keV. Rietveld refinement was run with RIQAS software (Materials Data Inc., Livermore, CA) to determine the lattice parameter of the HEB. Raman spectroscopy (Aramis Labram, Horiba Jobin Yvon, Edison, NJ) was performed using a He–Ne laser, no filter, 500 μm hole, and a slit size of 300 μm at 50× magnification. Oxygen content was measured using inert gas fusion (TC500, Leco, St. Joseph, MI).

2.3 | Mechanical Testing

Flexural strengths were measured in four-point bending using a fully-articulated test fixture and modified type-A bars (23.5 mm × 2.0 mm × 1.5 mm) at room temperature following ASTM C1161. Diamond grinding was performed on the top and bottom surfaces of the dense billets using a surface grinder (FSG-3A818, Chevalier, Santa Fe Springs, CA) with a ~15 μm diamond wheel. Electrical discharge machining (150HSS, Agie, Geneva, Switzerland) was used to initially cut the flexure bars out of the billets. Test bar tensile surfaces, aligned to be perpendicular to the SPS pressing direction, were polished using an automatic polisher to a 0.25 μm finish and chamfered by hand using a 3 μm diamond abrasive. A crosshead rate of 0.2 mm/min was used to test the bars. The lower span was 20 mm, while the upper span was 10 mm for the test fixture.

Fracture toughness was measured by the chevron notch method in four-point bending using a semi-articulated test fixture and modified type-A bars (23.5 mm × 3.0 mm × 4.0 mm) at room temperature according to ASTM Standard C1421 with 5 bars tested. The crosshead rate used was 0.0045 mm/min, which is adjusted from the standard to account for the bars shortened length and to maintain the same strain rate. A dicing saw (Accu-cut 5200; Aremco Products, Ossining, NY) with a 0.006 inch thick (~ 0.15 mm) diamond wafering blade was utilized to machine the chevron notches. A digital microscope (KH-8700; Hirox-USA, Hackensack, New Jersey) was used to measure the notch dimensions after testing.

Vickers indentation (ASTM C1327) was used to measure hardness at a load of 1.96 N and a dwell time of 10 s. Ten indents were measured for each specimen. The static bending method (ASTM E111) was used to measure elastic modulus during four-point bending tests. The deflection at the center point of the beam was measured with the assumption that the bottom load train was more rigid than the specimen.

3 | RESULTS AND DISCUSSION

3.1 | Powder synthesis, density, and microstructure

Nominally single-phase HEB ceramics were produced. The XRD patterns for the post-reacted powder, and after crushing a billet after SPS to produce a post-processed powder, are shown in Figure 1. No oxide peaks were detected in the reacted powder, but an incomplete solid solution was apparent based on the presence of multiple AlB_2 phases. The XRD pattern after SPS was indexed to the AlB_2 structure, with the lattice parameters being determined by Rietveld refinement to be $a = 3.0903$ Å and $c = 3.3509$ Å. After sintering, solid solution formation appeared to be complete, resulting in a single phase detected by XRD. The oxygen content of the sintered HEB ceramic was 0.06% ± 0.01%.

The HEB billet was near full density with a uniform grain size, as shown in the representative microstructure in Figure 2. The average grain size was 6 ± 2 μm with the largest grains measured to be ~17 μm. The aspect ratio of the grains was 1.5 ± 0.4. Small amounts (< 0.25 vol%) of excess carbon and boron carbide (indicated by arrows in Figure 2) were detected by Raman spectroscopy (not shown) at the grain boundaries. A small amount (< 0.25 vol%) of the oxide phase was also observed by SEM at the grain boundaries (indicated by arrows in

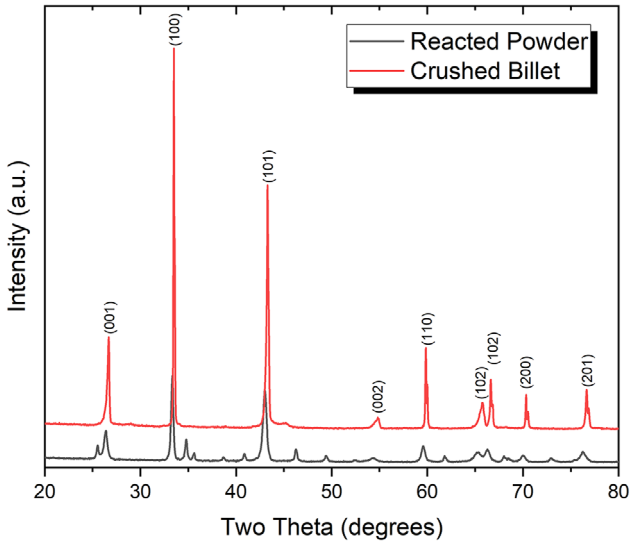

FIGURE 1 X-ray diffraction (XRD) of post reacted powder and crushed billet

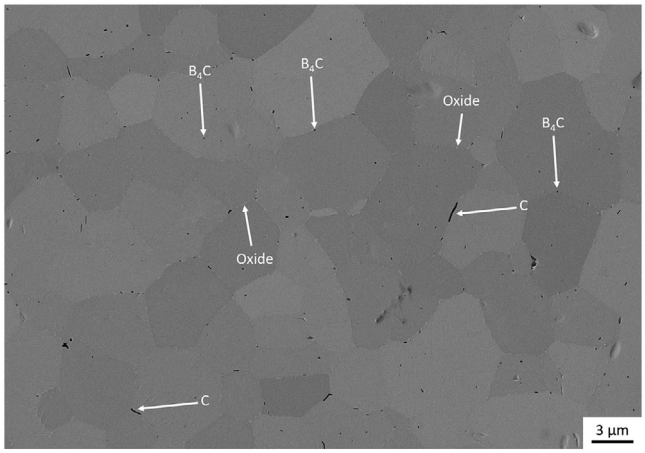

FIGURE 2 Representative polished microstructure of high-entropy boride (HEB). Arrows point to residual C, B_4C, and oxide within the microstructure

Figure 2). Figure 3 shows EDS maps of the microstructure, which indicate a uniform distribution of the metal elements. Based on Rietveld refinement using the lattice parameters from the X-ray diffraction pattern, the theoretical density was calculated to be 8.87 g/cm^3. Additionally, the average metallic molar mass based on the nominal batched composition was used in the theoretical density calculation. The bulk density was 8.98 g/cm^3 using the Archimedes method, with an apparent porosity of 0%. The measured bulk density was slightly higher than the calculated theoretical density, which is most likely due to the loss of some of the metals from the composition as volatile oxide species during the reaction process.[12] A small volume fraction (< 0.25 vol%) of oxide inclusions was observed in SEM, which is consistent with the measured oxygen content.

3.2 | Mechanical properties

Mechanical properties for the HEB produced in this study were measured at ambient conditions, and the results are summarized in Table 1. The static Young's modulus was measured in four-point bending to be 520 ± 12 GPa. A rule of mixtures calculation for each of the single-component diborides was used to estimate the Young's modulus for the HEB to be 501 ± 74 GPa, which is within 4% of the measured modulus of the ceramic.[13–18] The modulus of the HEB is higher than the modulus for WB_2 at 360 GPa, and close to the modulus of HfB_2 at 498 GPa.[14,16] ZrB_2,

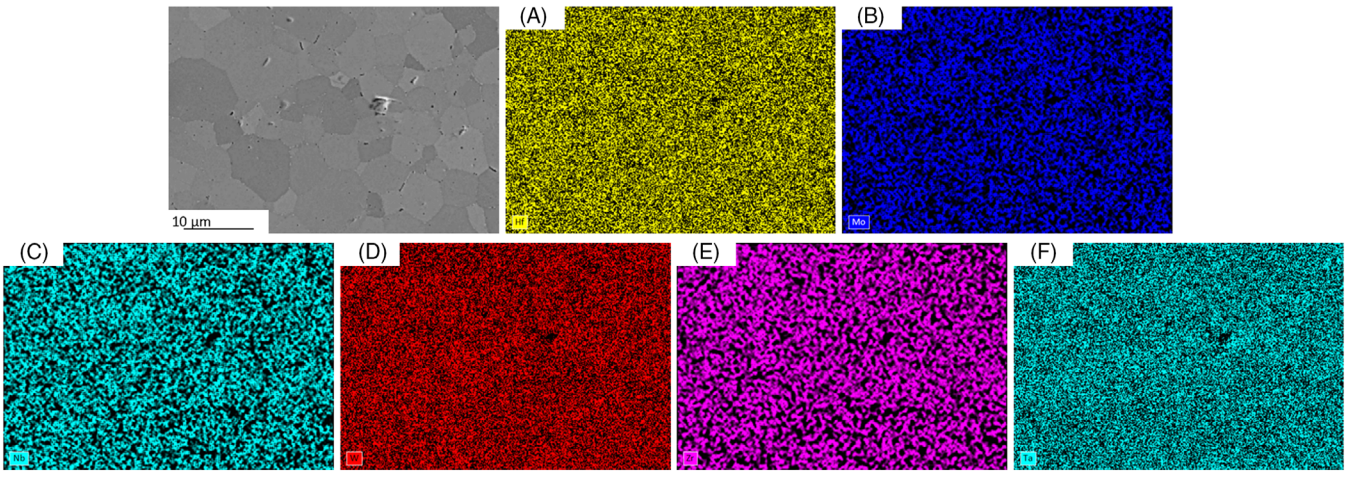

FIGURE 3 Scanning electron microscopy (SEM) image of high-entropy boride (HEB), and energy-dispersive spectroscopy (EDS) elemental maps of (A) Hf, (B) Mo, (C) Nb, (D) W, (E) Zr, and (F) Ta

TABLE 1 Summary of mechanical properties of high-entropy boride (HEB)

Density (g/cm^3)	Grain size (μm)	Young's modulus (GPa)	Hardness (GPa)	Strength (MPa)	Fracture toughness ($MPa \cdot m^{½}$)
9.05	6.2 ± 2.3	520 ± 12	32.1	528 ± 53	3.9 ± 1.2

TaB_2, NbB_2, and MoB_2 all have higher reported moduli at 519, 551, 512, and 569 GPa, respectively.[13–15,18] Modulus values for MoB_2 and WB_2 were obtained from calculated values, while the remaining diborides were experimentally determined. Feng et al. reported Young's modulus for an $(Nb,Hf,Ta,Ti,Zr)B_2$ ceramic to be 544 GPa measured using the impulse excitation method.[19] Feng's measured Young's modulus was slightly higher than the calculated value of ~ 529 ± 28 GPa.

Vickers hardness for the HEB was 33.1 ± 1.1 GPa for a 1.96 N load. Hardness values of 21.0 GPa for a $(Cr,Hf,Ta,Ti,Zr)B_2$ HEB and 28.3 GPa for a $(Cr,Hf,Ta,Ti,Zr)B_2$ HEB have been reported.[1,5] Hardness data for each of the individual diborides were reported to be 23 GPa, 26 GPa, 28 GPa, 24.4 GPa, 22.7 GPa, and 22.6 GPa for ZrB_2, TaB_2, HfB_2, MoB_2, NbB_2, and WB_2, respectively.[14, 18, 20–22] While each diboride reported had differences in density, and grain size, as well as the Vickers hardness indentation load used compared to the present work, the 33.1 GPa hardness for this six-component HEB is higher than any of the component diborides. To the best of the author's knowledge, this is the first report of hardness for a six-component HEB. The solid solution in the HEB appears to improve the Vickers hardness of the material, but further analysis is required to understand this behavior. Feng et al. measured the hardness of a variety of HEBs at a 1.96N load to be 25.2 GPa for a $(Hf,Nb,Ti,Ta,Zr)B_2$, 30.6 GPa for $(Hf,Mo,Ti,Ta,Zr)B_2$, 34.8 GPa for $(Hf,Ti,Ta,W,Zr)B_2$, and 30.9 GPa for $(Hf,Mo,Ti,W,Zr)B_2$.[8] While the compositions for the Feng et al. study differ from the present study, the overall hardness values are consistent with the present study. Qin et al. reported that HEBs containing WB_2 and MoB_2 were harder than HEBs not containing these diborides.[23] None of the HEBs for Feng et al. contained both WB_2 and MoB_2 which might be part of the reason for the higher hardness in the present work compared to Feng's work.

Figure 4 shows the radial-median cracks outlet from the corner of a Vickers diamond indent. The cracks appear to follow a transgranular crack propagation path. Neuman et al. reported crack propagation being predominately transgranular for a $(Zr_{0.96}W_{0.04})B_2$ ceramic and Dorner et al. also reported similar behavior for a $(Zr_{0.96}Ta_{0.04})B_2$ ceramic.[24,25] Zhang reported observing transgranular fracture in various HEBs due to a strong interface being formed at the grain boundaries.[5] The fracture mode observed in the HEB ceramic is comparable to other studies and indicates that the grain boundaries are strong relative to the grains.

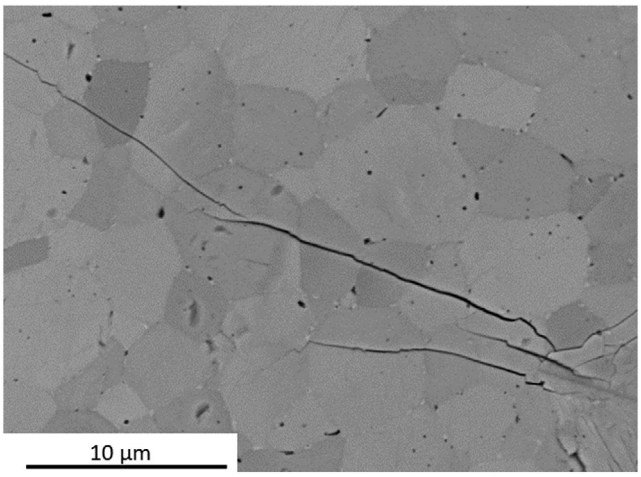

FIGURE 4 Crack path starting from the corners of a Vickers indent

Flexural strength and fracture toughness for the $(Hf,Mo,Nb,Ta,W,Zr)B_2$ ceramic in the present study were 528 ± 53 MPa and 3.9 ± 1.2 $MPa \cdot m^{1/2}$, respectively. This is one of the first reports for flexure strength and fracture toughness of a six-component HEB ceramic. Liu et al. reported the four-point bend strength of a $(HfNbTaTiZr)B_2$ to be 339 ± 17 MPa and the fracture toughness to be 3.8 ± 0.4 $MPa \cdot m^{1/2}$ using the single-edge notched beam technique.[9] The average grain size for Liu's material was 4 µm which is close to the average grain size in the present work. While Liu's strength is significantly lower than the strength measured in the present study, the fracture toughness was within a few percent. Additionally, Liu had a higher amount of oxide impurity within the material compared to the present study, which may have caused the difference in strength. Thompson et al. reported the strengths for ZrB_2 as a function of grain size and for similar-sized grains as the present work (~ 7 µm) to be ~ 430 to 445 MPa.[26] The strengths in the present work are higher than ZrB_2 with the same grain size reported by Thompson, indicating that some strengthening mechanism may be active in the HEB, the type of flaw causing failure is different, or both. Additionally, it does not appear that fracture toughness of the HEB ceramic in the present study benefits from the solid

solution formation, as its fracture toughness falls into the range for the component borides (2–5 MPa·$m^{1/2}$).[13,20,27]

A Griffith-type analysis was utilized for estimating the critical flaw sizes of the HEB material. Since the secondary oxide phase and residual carbon and boron carbide phases were significantly smaller than the average grain size of the HEB phase, they should not be the strength limiting flaw in the material. The crystal structure of the HEB ceramic produced in this study is hexagonal, and as such can be susceptible to microcracking if the coefficients of thermal expansion (CTE) for the *a*,*b*-axes versus *c*-axis are substantially different. CTE was not measured for this material, but Watts et al. reported the grain size required for microcracking in pure ZrB_2 to be ~980 μm which is significantly larger than the largest grain measured in this material.[28] Further, microcracking was not observed in the microstructure of the HEB. The Y crack geometry constants for the Griffith analysis were selected based on the measured aspect ratios of the grains, as outlined in ASTM C1322. Different Y crack geometry constants were used based on the grain aspect ratios, which were in the range from $c = 1.4a$ ($Y = 1.39$) to $c = 2.0a$ ($Y = 1.59$). The critical flaw sizes calculated for these Y parameters were 28 ± 17 μm and 21 ± 13 μm, respectively. The largest grains measured were ~ 17 μm which fits reasonably well for both stress intensity factor flaw size calculations. As such, the critical flaw of the material is likely the largest grains. Therefore, decreasing the size of the largest grains would increase the strength of the material.

4 | SUMMARY

A nominally phase pure (Hf,Mo,Nb,Ta,W,Zr)B_2 high-entropy diboride ceramic was produced. The HEB was sintered to near full density (8.98 g/cm^3) at 2000°C. The average grain size was 6 ± 2 μm with a maximum grain size of 17 μm. Small amounts of carbon and B_4C were still present in the microstructure, along with a secondary oxide phase being found at the grain boundaries. The room-temperature mechanical properties of the (Hf,Mo,Nb,Ta,W,Zr)B_2 were measured; flexural strength was 528 ± 53 MPa, Young's modulus was 520 ± 12 GPa, fracture toughness was 3.9 ± 1.2 MPa·$m^{1/2}$, and hardness ($HV_{0.2}$) was 33.1 ± 1.1 GPa. This is one of the first reports of the mechanical properties of a six-component HEB ceramic. A Griffith-type analysis was utilized and determined the strength-limiting flaw of the HEB material to be the largest grains in the microstructure. Further study into other HEB compositions could provide insight into which elements lead to the enhanced strength and hardness of the HEB compared to lower strength and hardness values measured for other borides with comparable grain sizes containing either one transition metal or different combinations of transition metals.

ACKNOWLEDGMENTS

The authors would like to thank the Missouri S&T Advanced Characterization Laboratory for assistance with specimen characterization. Funding for the project was provided by GE Research under the project "Chemical Compatibility of Refractory High Entropy Alloys with Ultra-High Temperature Ceramics." The authors would like to thank program manager Andrew Detor for his support on this work.

REFERENCES

1. Gild J, Zhang Y, Harrington T, Jiang S, Hu T, Quinn MC, et al. High-entropy metal diborides: A new class of high-entropy materials and a new type of ultrahigh temperature ceramics. Sci Rep. 2016;6(October):37946. Available from: http://www.nature.com/articles/srep37946
2. Tallarita G, Licheri R, Garroni S, Orru' R, Cao G. Novel processing route for the fabrication of bulk high-entropy metal diborides. Scr Mater. 2019;158:100–4. Available from: https://doi.org/10.1016/j.scriptamat.2018.08.039
3. Liu D, Wen T, Ye B, Chu Y. Synthesis of superfine high-entropy metal diboride powders. Scr Mater. 2019;167:110–4. Available from: https://doi.org/10.1016/j.scriptamat.2019.03.038
4. Wen T, Ning S, Liu D, Ye B, Liu H, Chu Y. Synthesis and characterization of the ternary metal diboride solid-solution nanopowders. J Am Ceram Soc. 2019;102(8):4956–62.
5. Zhang Y, Guo WM, Jiang ZB, Zhu QQ, Sun SK, You Y, et al. Dense high-entropy boride ceramics with ultra-high hardness. Scr Mater. 2019;164:135–9. Available from: https://doi.org/10.1016/j.scriptamat.2019.01.021
6. Zhang Y, Jiang ZB, Sun SK, Guo WM, Chen QS, Qiu JX, et al. Microstructure and mechanical properties of high-entropy borides derived from boro/carbothermal reduction. J Eur Ceram Soc. 2019;39(13):3920–4. Available from: https://doi.org/10.1016/j.jeurceramsoc.2019.05.017
7. Feng L, Fahrenholtz WG, Hilmas GE. Two-step synthesis process for high-entropy diboride powders. J Am Ceram Soc. 2020;103(2):724–30.
8. Feng L, Monteverde F, Fahrenholtz WG, Hilmas GE. Superhard high-entropy AlB2-type diboride ceramics. Scr Mater. 2021;199:113855. Available from: https://doi.org/10.1016/j.scriptamat.2021.113855
9. Liu Jx, Shen Xq, Wu Y, Li F, Liang Y, Zhang Gj. Mechanical properties of hot-pressed high-entropy diboride-based ceramics. J Adv Ceram. 2020;9(4):503–10.
10. Chamberlain AL, Fahrenholtz WG, Hilmas GE. Pressureless sintering of zirconium diboride. J Am Ceram Soc. 2006;89(2):450–6. Available from: http://doi.wiley.com/10.1111/j.1551-2916.2005.00739.x
11. Zhang SC, Hilmas GE, Fahrenholtz WG. Pressureless densification of zirconium diboride with boron carbide additions. J Am Ceram Soc. 2006;89(5):1544–50.
12. Hinshelwood CN, Blackburn PE, Hoch M, Johnston HL. The vaporization of molybdenum and tungsten oxides. J Phys

Chem. 1958;62(7):769–73. Available from: https://doi.org/10.1021/j150565a001

13. Fahrenholtz WG, Wuchina EJ, Lee WE, Zhou Y. Ultra-high temperature ceramics: Materials for extreme environment applications. 2014.
14. Zhang X, Hilmas GE, Fahrenholtz WG. Synthesis, densification, and mechanical properties of TaB2. Mater Lett. 2008;62(27):4251–3.
15. Regalado E, Escamilla R. Elastic properties of superconducting NbB 2+ *x* obtained from first-principles calculations. J Phys Condens Matter. 2007;19(37):376209.
16. Zhao E, Meng J, Ma Y, Wu Z. Phase stability and mechanical properties of tungsten borides from first principles calculations. Phys Chem Chem Phys. 2010;12(40):13158–65.
17. Liang Y, Yuan X, Fu Z, Li Y, Zhong Z. An unusual variation of stability and hardness in molybdenum borides. Appl Phys Lett. 2012;101(18):181908. Available from: https://doi.org/10.1063/1.4764547
18. Zhang M, Wang H, Wang H, Cui T, Ma Y. Structural modifications and mechanical properties of molybdenum borides from first principles. J Phys Chem C. 2010;114(14):6722–5.
19. Feng L, Fahrenholtz WG, Hilmas GE, Monteverde F. Effect of Nb content on the phase composition, densification, microstructure, and mechanical properties of high-entropy boride ceramics. J Eur Ceram Soc. 2021;41(1):92–100. Available from: https://doi.org/10.1016/j.jeurceramsoc.2020.08.058
20. Fahrenholtz WG, Hilmas GE, Talmy IG, Zaykoski JA. Refractory diborides of zirconium and hafnium. J Am Ceram Soc. 2007;90(5):1347–64.
21. Otani S, Korsukova MM, Mitsuhashi T. Floating zone growth and high-temperature hardness of NbB2 and TaB2 single crystals. J Cryst Growth. 1998;194(3–4):430–3.
22. Okada S, Atoda T, Higashi I, Takahashi Y. Preparation of single crystals of MoB_2 by the aluminium-flux technique and some of their properties. J Mater Sci. 1987;22(8):2993–9.
23. Qin M, Gild J, Wang H, Harrington T, Vecchio KS, Luo J. Dissolving and stabilizing soft WB2 and MoB2 phases into high-entropy borides via boron-metals reactive sintering to attain higher hardness. J Eur Ceram Soc. 2020;40(12):4348–53.
24. Neuman EW, Fahrenholtz WG, Hilmas GE. Microstructure and mechanical properties of reaction-hot-pressed zirconium diboride based ceramics. Int J Appl Ceram Technol. 2019;16(April):1715–22. Available from: https://doi.org/10.1111/ijac.13263
25. Dorner AN, Werbach K, Hilmas GE, Fahrenholtz WG. Effect of tantalum solid solution additions on the mechanical behavior of ZrB2. J Eur Ceram Soc. 2021;41(6):3219–26. Available from: https://doi.org/10.1016/j.jeurceramsoc.2020.12.049
26. Thompson M, Fahrenholtz WG, Hilmas GE. Effect of starting particle size and oxygen content on densification of ZrB2. J Am Ceram Soc. 2011;94(2):429–35.
27. Fahrenholtz WG, Hilmas GE. Oxidation of ultra-high temperature transition metal diboride ceramics. Int Mater Rev. 2012;57(1):61–72.
28. Watts J, Hilmas G, Fahrenholtz WG. Mechanical characterization of ZrB_2–SiC composites with varying SiC particle sizes. J Am Ceram Soc. 2011;94(12):4410–8.

How to cite this article: Murchie AC, Watts JL, Fahrenholtz WG, Hilmas GE. Room-temperature mechanical properties of a high-entropy diboride. Int J Appl Ceram Technol. 2022;19:2293–2299. https://doi.org/10.1111/ijac.14026